NASA Conference Publication 2338

Proc., Rotordynamic Instability Problems in

High-Performance Turbomachinery,

May 28-30, 1984, Texas A & M Univ., College Station,

Texas, p. 109-122

Lateral Fluid Forces Acting on a Whirling Centrifugal Impeller in Vaneless and Vaned Diffuser

Ohashi, H. and Shoji, H.

LATERAL FLUID FORCES ACTING ON A WHIRLING CENTRIFUGAL IMPELLER IN VANELESS AND VANED DIFFUSER*

Hideo Ohashi
University of Tokyo
Tokyo 113, Japan

Hidenobu Shoji
Tsukuba University
Ibaragi-ken 305, Japan

Fluid forces on a rotating centrifugal impeller in whirling motion were studied experimentally. A two-dimensional impeller installed in a parallel-walled vaneless and vaned diffuser whirled on a circular orbit with various positive and negative angular velocities. The results showed that the fluid forces exert a damping effect on the rotor in most operating conditions, but become excitatory when the impeller operates at very low partial discharge while rotating far faster than the whirl speed.

The fluid forces were also expressed in terms of mass, damping and stiffness matrices. Calculations were conducted for impellers with the same geometry and whirl condition as those in the experiment. Quantitative agreement was obtained especially in positive whirl.

INTRODUCTION

As to fluid forces acting on a centrifugal impeller of pumps and compressors, many studies have been done on the steady lateral forces (radial thrust), which occur either by azimuthally asymmetric configuration of volute casing or by misalignment of impeller and casing center. To the contrary, limited contributions have been made to the unsteady part of lateral forces, which is induced by the whirling motion of rotating impellers. This is the very information sought for the precise analysis of rotor stability and seismic response.

Experimental study on this subject is quite few. Two projects are presently under way as far as known to the authors, one at California Institute of Technology and the other at University of Tokyo.

The latter, i.e. the present experimental study is the direct counterpart to the theoretical calculation reported at the 1st Workshop [ref. 1]. Therefore the geometries of the test impeller and casing were determined to be similar to those of sample calculations. This is the reason why this experiment adopted deliberately much simpler configurations than those of actual pumps and compressors. The project at CIT seems to lay more stress on the practical side than we intend, because the adopted impeller/casing configuration is similar to those of pumps for industrial application. The progress of CIT project was reported twice at the 1st and 2nd Workshop by Acosta et al. [ref. 2, 3].

---

* This study was supported by Grant in Aid for Scientific Research by the Ministry of Education, Technical Research Institute for Integrity of Structures at Elevated Service Temperatures and Hitachi, Ltd. Messrs. S. Yanagisawa, K. Tomita, J. Hanawa, K. Kawakami and C. Kato contributed to this study as their Master theses.

TEST FACILITY

The test pump is a single-stage, vertical shaft, centrifugal type. The mechanism of the forced whirling motion is illustrated schematically in fig. 1. The impeller is supported overhung by two self-alignment roller bearings, which are mounted separately on the upper and lower whirl plates. Fluid forces acting on the impeller are evaluated from the reaction force to the lower bearing. As seen from fig. 1, the outer race of the lower bearing is attached to the lower whirl plate by four load cells arranged with 90 degree angle difference (x- and y-direction).

Fig. 2 shows the relative arrangement of impeller and diffuser. In order to avoid the generation of steady lateral forces, the flow passage was designed to ensure axisymmetric flow by means of resistance screen at the diffuser exit and two symmetrically arranged discharge pipes for instance. Test was conducted mainly for vaneless diffuser. Additional test was also done for vaned diffuser with 2, 4 and 8 guide vanes, though the corresponding theory had not been established for comparison. Two impellers, A and B, with different vane angle were tested. The rotational speed of the impeller shaft was kept constant (8.8 Hz), while the whirl speed was varied widely from negative to positive whirl. Both pump and eccentric drive shafts were equipped with rotary encoders to detect phase angle. Principal specifications of test pump are listed in table 1.

DATA EVALUATION

Calibration

The load cells were calibrated dynamically by a rotating disc with known unbalance mass. The conversion factors (a = impeller force (N)/load cell output (V)) were determined for the x- and y-direction separately. The linearity of the cells was satisfactory and all cross terms, output of y-cells to x-directed force for instance, remained less than two percent of their principal terms.

Data Aquisition

Outputs of load cells were A/D converted and stored by sampling signals generated at every 10 degree on whirling orbit. For experiment to check the statistical character of the data, ensemble average and rms were evaluated from 512 sampled data at the same condition. In other cases 200 to 300 data were collected to give an ensemble average with intended confidence interval. In the experiment with vaned diffuser, samplings were made when the phase angle of whirl and impeller shaft, θ_1 and θ_2 (cf. fig. 4(a)), coincided simultaneously with the preset values.

Evaluation of Fluid Forces on Impeller Vanes

Since the theoretical results which are to be compared with the experiment, consider only fluid forces acting on the impeller vanes, and exclude all other forces on shroud, shaft, seal etc, it is necessary also in the experiment to extract pure vane force from the resultant reaction force measured at the lower bearing. For this purpose, four experiments were carried as shown in fig. 3, that is, experiments with whirling impeller in water and in air, and with whirling dummy rotor in water and in air.

The fluid force on the impeller vanes, $F(F_x, F_y)$, can be evaluated by the relation,

$$F = a (E_1 - E_2 - E_3 + E_4) \qquad \text{.....(1)}$$

where $E_i(E_x, E_y)$ denotes load cell outputs in the above mentioned four sub-

experiments. The following interpretation will also help understand the meaning of eq. (1):

$a(E_1-E_2)$; fluid forces on whirling components submarged in water.

$a(E_3-E_4)$; fluid forces on whirling components submarged in water except vanes, i.e. those on shrouds, shaft and seal (see fig. 1).

The reaction of driving shaft torque on the lower bearing was calculated and the influence was compensated in the final evaluation of impeller force.

As seen from fig. 4 (a), fluid forces on whirling impeller are dependent of rotational speed ω, whirl speed Ω, eccentricity ε, phase angle of whirl θ_1 and rotation θ_2 and flow rate Q. The dependence on θ_2 disappers in vaneless diffuser.

Test Condition

The eccentricity was kept constant (ε = 1.5 mm), since linearity could be expected for such small displacement. From the rotordynamic consideration the whirl speed Ω corresponds to the first damped natural frequency in bending mode of the rotor (critical speed). Although most troubles associated with non-synchronous rotor vibration occur at supercritical rotational speed, $\Omega/\omega<1$, the test was done at whirl speed ratio Ω/ω up to 1.3 both for positive and negative whirl. Because impeller forces are sensitive to the operating condition of the impeller, discharge rate was varied from shutoff to maximum.

Presentation of Fluid Forces

Fluid forces F acting on the impeller vanes are divided into two components as illustrated in fig. 4 (b). The component normal to the orbit and directed outward is called radial force F_r, while the component parallel and opposite to the clockwise (positive) whirl is called tangential force F_θ. A negative sign means the direction is opposite to the above definition.

TEST RESULTS AND DISCUSSION

Pump Characteristics

The hydraulic performance of the test pump (impeller A and B) at steady operation is plotted in fig. 5 in non-dimensional form, in which flow coefficient ϕ and head coefficient ψ are defined by (see notation in table 1)

$$\phi = Q / 2\pi r_2 b u_2 , \quad u_2 = \omega r_2 \qquad \text{.....(2)}$$

$$\psi = H / (u_2^2/2g)$$

Since impeller B has smaller exit vane angle than that of A, it has larger work input and hence higher head. Guide vanes have logarithmic spiral form and the vane angle is set to have no loading at design (shock-free) discharge of the impeller. Because of this design principle, the influence of guide vanes on the steady performance is not remarkable. Design flow coefficient, at which the relative inlet flow to the impeller vanes becomes shock-free, is denoted by ϕ_{sf}.

The machine Reynolds number of the test pump, $Re = u_2 d_2/\nu$, was about 3.4×10^6 in all test cases.

Character of Unsteady Fluid Forces

Fluid forces acting on whirling vanes, F, are evaluated from four forces obtained by four sub-experiments (see eq. (1)). The relative magnitude and direction of these four forces are illustrated in fig. 6 for a typical test condition (impeller A, $\phi=\phi_{sf}$, ε=2 mm, Ω/ω=0.83 and θ_1=0). F_2 and F_4 measured in air are caused by inertial centrifugal force and thus have only radial component.

The effort to reduce the mass of whirling components by using aluminum helped keep the level of fluid force substantially larger than that of inertia force.

Outputs of load cells oscillate primarily with the whirl speed Ω, but contain also fluctuations caused by mass unbalance of impeller, rolling noise of bearings, noise of measuring system, turbulence of flow and so on. From the preliminary studies, it became clear that the largest and predominant source of data scattering resulted from the fluctuation of flow field in impeller and diffuser. Fig. 7 illustrates Lissajous figures of overall impeller force, when impeller A rotates in water without whirling motion. As seen from fig. 7 (a), fluctuation of measured force is rather trivial at design, i.e. shock-free discharge condition. As the discharge decreases, the fluctuation gets larger and at shutoff the fluctuation becomes quite violent as seen from fig. 7 (b). The reason is obviously the separation and large scale turbulence of the flow in impeller. The fluctuation of measured force can therefore be attributed mostly to the inherent flow turbulence.

Fig. 8 shows fluid forces on whirling impeller vanes at 9 locations of the orbit (impeller A, ε =1.5 mm , vaneless dif.) for the combination of two flow rates (design and shutoff) and two whirl speed ratios (positive and negative). Each vector indicates ensemble average of 512 sampled data, while the magnitude of fluctuation is indicated by a circle with rms as its radius. Fluid forces are nearly axisymmetric and uniform on the orbit as they should be. It is worth to note, that especially near shutoff the fluctuation in rms can be severalfold as high as its average.

Fluid Forces on Whirling Impeller in Vaneless Diffuser

In spite of precautions to establish azimuthally symmetric flow, the ensemble averaged force vectors on the orbit were not completely uniform as seen from fig. 8. Since the influence of fluid forces on the dynamics of rotor is accumulative, the force components, F_r and F_θ, are hereafter averaged over one cycle of whirl angle θ_1 and shaft angle θ_2, and are denoted by $\overline{F}_r$ and $\overline{F}_\theta$. These forces are further normalized by the following definitions;

$$f_r = \overline{F}_r / M\varepsilon\omega^2, \qquad f_\theta = \overline{F}_\theta / M\varepsilon\omega^2 \qquad \text{.....(3)}$$

$$M = \rho\pi r_2^2 b$$

where ρ is the density of the working fluid and M is the mass of fluid displaced by the silhouette volume of impeller vanes.

Fig. 9 shows the dependence of f_r and f_θ on the whirl speed ratio Ω/ω from -1.3 to +1.3, when impeller A (β=68°) whirls with eccentricity ε =1.5 mm in vaneless diffuser and operates at five different flow rates from shutoff to maximum. The broken line in the figure indicates calculated result for shock-free entry condition ($\phi=\phi_{sf}$). Fig. 10 shows the corresponding result of impeller B (β=60°).

As to radial component followings can be observed: 1) The apparent mass of impellers A and B is about 0.9 and 0.7 times displaced fluid mass M, respectively, when it merely oscillates without rotation. Therefore, if there is no influence of pumping action on the fluid forces, f_r must be equal to $0.9\times(\Omega/\omega)^2$ for impeller A and $0.7\times(\Omega/\omega)^2$ for impeller B. The calculated f_r at shock-free entry agrees with this simple prediction quantitatively in positive whirl, but becomes almost twice as large as the prediction in negative whirl. It suggests that the pumping impeller in negative whirl has a certain flow mechanism to generate large radial force even in potential theory. 2) At design discharge, that is, shock-free entry condition, the measured radial forces agree with the theory well in tendency. In positive whirl quantitative agreement is fairly good, while in negative whirl the measurement is remarkably larger than the theory. 3) Radial force decreases as discharge decreases in positive whirl.

In negative whirl the tendency is quite opposite. 4) At and near $\Omega/\omega=1.0$, where the relative flow in impeller becomes stationary, radial force becomes negative at very low discharge. 5) At $\Omega/\omega=0$ (stationary displacement), rotating impeller produces positive radial force, that is, force to the direction of impeller displacement. This means that radial fluid force has negative-spring characteristics. 6) Impeller A has slightly larger radial force than that of impeller B.

As to tangential component: 1) Except a few test conditions, tangential forces are positive in positive whirl and negative in negative whirl. This indicates that fluid forces exert a damping effect on whirling impeller in most cases. 2) Negative tangential force emerges in positive whirl when the pump operates at very low discharge while rotating more than twice as fast as whirl speed ($\Omega/\omega<0.5$). In this condition the fluid force feeds energy to the whirling system and can cause a self-excited oscillation, a sort of impeller whip. 3) The agreement with theory is good in positive whirl. In negative whirl the measurement is again remarkably higher than the theory predicts. 4) In negative whirl larger damping can be expected than in positive whirl. 5) The influence of discharge rate on tangential component is generally small.

Influence of Guide Vanes on Rotor Stability

Since the radial clearance between impeller and guide vanes was chosen relatively large (11% of radius), the hydrodynamic interference of guide vanes to impeller vanes was so limited that the dependence of impeller force on the phase angle of impeller shaft, θ_2, was undetectably small. Consequently the installation of guide vanes resulted in little difference of the mean components of fluid forces from those given in fig. 9 and 10.

Guide vanes augmented the damping effect on the rotor stability to some extent. For the convenience of stability judgement, a new normalized parameter of tangential force is introduced as

$$f_\theta' = \overline{F}_\theta / M \varepsilon \Omega \omega \qquad \text{.....(4)}$$

According to this definition small f_θ at small whirl speed ratio Ω/ω can be enlarged by dividing by Ω. f_θ' has also the feature that it keeps positive throughout positive and negative whirl range, as far as the fluid force exerts damping effect. Fig. 11 shows f_θ' of impeller A at various flow rates, when it whirls in vaneless (no GV) and vaned diffuser with 2 and 8 guide vanes. In the case of vaneless diffuser, theoretical prediction for shock-free entry condition is also plotted by broken lines. From these figures it is evident that guide vanes reduce the range of whirl speed ratio with negative f_θ', thus resulting in increased damping on the whirling rotor.

Comparison with Theory by Vector Diagram

Fluid forces at shock-free entry condition are compared with the theoretical result [ref. 1] using vector diagrams as shown in fig. 12. Normalized force vectors are plotted with whirl speed ratio Ω/ω as their parameter on the curves. Theoretical and experimental curves coincide fairly well as a shape of curves but there is a considerable difference of the location of parameters. This difference could be caused either by the viscous effect neglected in this theory or by unaware factors hidden in the test setup and instrumentation.

CONVERSION TO MATRIX ELEMENTS

In the analysis of rotor dynamics it is convenient to express fluid forces in terms which are proportional to the displacement, velocity and acceleration of impeller center. As illustrated in fig. 4 (a), the location of impeller

center O(x, y) is expressed by the absolute coordinate system with its origin at the whirl center O'. Denoting x- and y-components of fluid forces by F_x and F_y, they are expressed in the following linear form;

$$\begin{bmatrix} F_x \\ F_y \end{bmatrix} = -\underbrace{\begin{bmatrix} m_{xx} & m_{xy} \\ m_{yx} & m_{yy} \end{bmatrix}}_{\text{mass}} \begin{bmatrix} \ddot{x} \\ \ddot{y} \end{bmatrix} - \underbrace{\begin{bmatrix} b_{xx} & b_{xy} \\ b_{yx} & b_{yy} \end{bmatrix}}_{\text{damping}} \begin{bmatrix} \dot{x} \\ \dot{y} \end{bmatrix} - \underbrace{\begin{bmatrix} k_{xx} & k_{xy} \\ k_{yx} & k_{yy} \end{bmatrix}}_{\text{stiffness}} \begin{bmatrix} x \\ y \end{bmatrix} \quad \text{.....(5)}$$

where $x = \varepsilon \cos\theta_1$, $y = \varepsilon \sin\theta_1$ and $\theta_1 = -\Omega t$.

Because the measured fluid forces are non-linear with respect to location, velocity and acceleration of impeller center, it is impossible to determine the above matrix elements in an exact meaning. However, if the fluid forces are axisymmetric on the whirling orbit (independent of θ_1), and can be approximated by the equations

$$F_r(\varepsilon, \Omega) = \varepsilon (F_{r0} + F_{r1}\Omega + F_{r2}\Omega^2) \quad \text{.....(6)}$$

$$F_\theta(\varepsilon, \Omega) = \varepsilon (F_{\theta 0} + F_{\theta 1}\Omega + F_{\theta 2}\Omega^2)$$

the matrix elements can be related to the above terms as;

$$\begin{aligned} m_{xx} &= m_{yy} = F_{r2}, \quad m_{xy} = -m_{yx} = -F_{\theta 2} \\ b_{xx} &= b_{yy} = F_{\theta 1}, \quad b_{xy} = -b_{yx} = F_{r1} \\ k_{xx} &= k_{yy} = -F_{r0}, \quad k_{xy} = -k_{yx} = F_{\theta 0} \end{aligned} \quad \text{.....(7)}$$

The fitting of measured data to eq. (6) can be performed by applying the method of least squares.

Fig. 13 shows the fitted curve of impeller A at shock-free condition. The fitting was made for all data in positive and negative whirl, $-1.3 < \Omega/\omega < +1.3$. Since the real fluid forces are non-linear, the fitted curve cannot represent the measured data satisfactorily in the whole whirl speed ratio. Especially the delicate change of fluid forces near $\Omega/\omega = 1$ is neglected in the fitting completely. The quality of fitting deteriorates gradually as flow rate decreases and the flow in impeller deviates from shock-free condition.

Fig. 14 illustrates the fitted curves of impeller A in vaneless diffuser at various flow rates. As seen from the figure tangential force f_θ changes almost linearly with whirl speed ratio. This indicates that cross mass term $m_{xy}=-m_{yx}$ is insignificant. The feature of radial force f_r consists in the fact that it is parabolic in general but the minimum takes place around $\Omega/\omega=0.4$. This result infers that cross damping term $b_{xy}=-b_{yx}$ plays an important role.

In table 2 and 3 matrix elements of impeller A and B in vaneless diffuser are listed for various flow rates. All values are normalized by the quantities given in the tables.

CONCLUSION

Fluid forces acting on two-dimensional centrifugal impeller whirling in vaneless and vaned diffuser were measured and compared with the corresponding theoretical results. Principal findings from two tested impellers are:

1) Fluid forces have tangential components to damp whirling motion of the rotating shaft in most operating condition.

2) At low flow rate near shutoff and low whirl speed ratio, i.e. at high supercritical rotational speed, there are possibilities that the fluid forces do exert negative damping to the rotor in positive whirl, a sort of impeller whip.
3) Theoretical calculation can predict fluid forces qualitatively. Quantitative agreement can be obtained in positive whirl.
4) Fluid forces are expressed as elements of mass, damping and stiffness matrices by assuming linear relation.

This study will be extended further to the cases in which impeller whirls in a volute casing. The 2nd generation test rig with improved whirling mechanism, instrumentation and versatile applicability is under construction.

LITERATURES

1. Shoji, H. and Ohashi, H., "Fluid Forces on Rotating Centrifugal Impeller with Whirling Motion," NASA Conference Publication 2133, 1980, p. 317-328.
2. Brennen, C.E., Acosta, A.J. and Caughey, T.K., "A Test Program to Measure Fluid Mechanical Whirl-Excitation Forces in Centrifugal Pumps," NASA CP 2133, 1980, p. 229-235.
3. Chamieh, D.S. et al, "Experimental Measurements of Hydrodynamic Stiffness Matrices for a Centrifugal Pump Impeller," NASA CP 2250, 1982, p. 382-398.

Table 1 Principal specifications

Impeller	Two-dimensional, closed type
outer diameter $d_2=2r_2$	350 mm
inner diameter	175 mm
vane width b	35 mm
suction diameter	160 mm
number of vanes	6
vane angle to radius β (logarithmic spiral)	68° for impeller A 60° for impeller B
mass	4.1 kg
Vaneless diffuser	Parallel walled
exit diameter	700 mm
screen	40 mesh per inch, 51% opening
width	70 mm
Vaned diffuser	Logarithmic spiral, 5 mm thickness
inner diameter	390 mm (20 mm radial clearance)
outer diameter	600 mm
width	60 mm
number of vanes	2, 4 and 8
vane angle to radius	75.5°
Test condition	
rotational speed ω	525 rpm
whirl speed Ω	-683 to +683 rpm
eccentricity ε	variable, mainly 1.5 mm
shock-free flow rate	2.25 m^3/min for impeller A 3.21 m^3/min for impeller B

Table 2 Matrix elements of impeller A

matrix element	m_{xx}, m_{yy}	m_{xy},$-m_{yx}$	b_{xx}, b_{yy}	b_{xy},$-b_{yx}$	k_{xx}, k_{yy}	k_{xy},$-k_{yx}$
normalized by	$\pi\rho r_2^2 b$		$\pi\rho r_2^2 b\omega$		$\pi\rho r_2^2 b\omega^2$	
ϕ = 0	1.64	0.27	1.14	-2.02	-0.55	-0.13
0.2 ϕ_{sf}	1.72	0.35	1.10	-2.01	-0.55	-0.17
0.6 ϕ_{sf}	1.87	0.32	1.08	-1.88	-0.56	-0.10
ϕ_{sf}	1.86	0.27	0.98	-1.33	-0.42	0.09
1.3 ϕ_{sf}	1.82	0.23	1.09	-1.01	-0.43	0.08

Table 3 Matrix elements of impeller B

matrix element	m_{xx}, m_{yy}	m_{xy},$-m_{yx}$	b_{xx}, b_{yy}	b_{xy},$-b_{yx}$	k_{xx}, k_{yy}	k_{xy},$-k_{yx}$
normalized by	$\pi\rho r_2^2 b$		$\pi\rho r_2^2 b\omega$		$\pi\rho r_2^2 b\omega^2$	
ϕ = 0	1.30	0.21	0.98	-1.98	-0.58	-0.12
0.2 ϕ_{sf}	1.32	0.33	0.94	-1.96	-0.57	-0.17
0.6 ϕ_{sf}	1.26	0.20	1.06	-1.80	-0.43	-0.13
ϕ_{sf}	1.34	0.19	1.01	-1.62	-0.39	-0.05
1.3 ϕ_{sf}	1.32	0.05	1.00	-1.35	-0.35	0.01

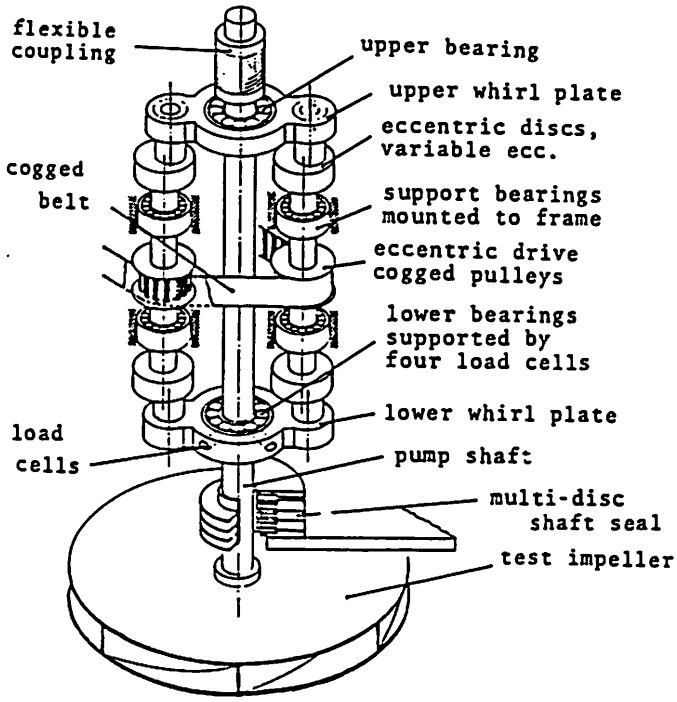

Fig. 1 Whirling mechanism

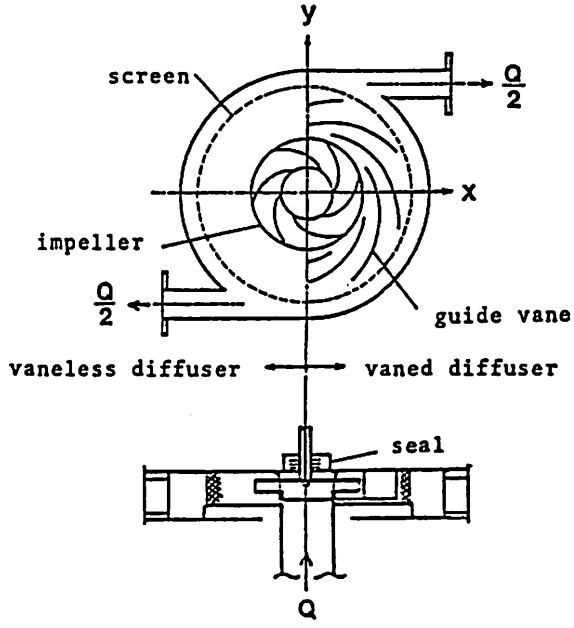

Fig. 2 Configuration of impeller and diffuser

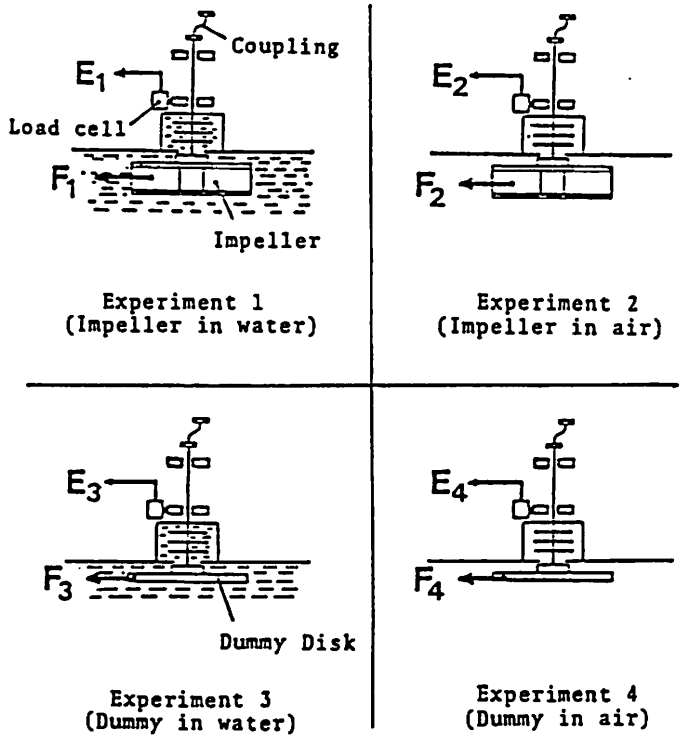

Fig. 3 Four sub-experiments

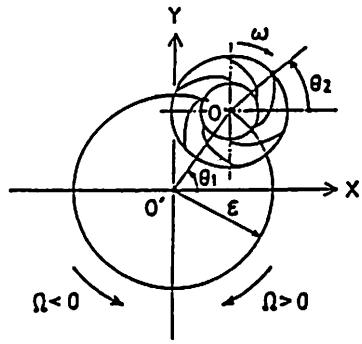

(a) Coordinates

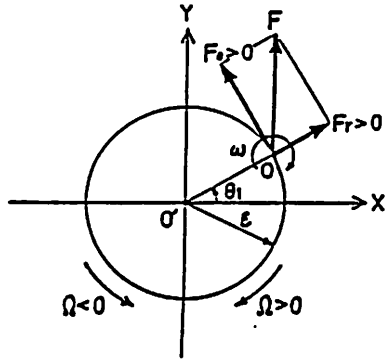

(b) Force vector

Fig. 4 Notations

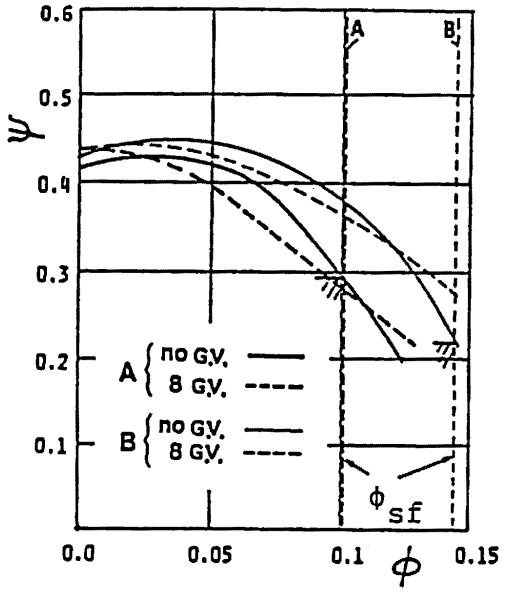

Fig. 5 Characteristics of test pumps

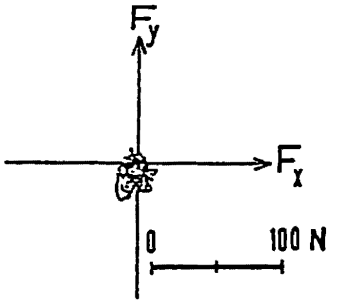

(a) $\phi = \phi_{sf}$

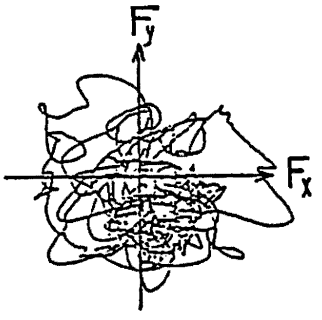

(b) $\phi = 0$

Fig. 7 Time histories of fluid force vector

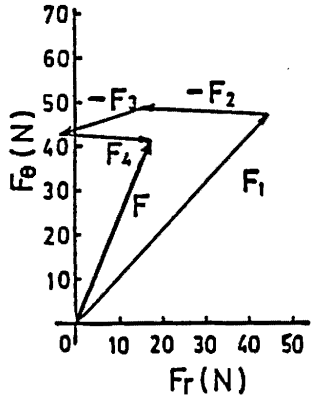

Fig. 6 Relative disposition of force vectors

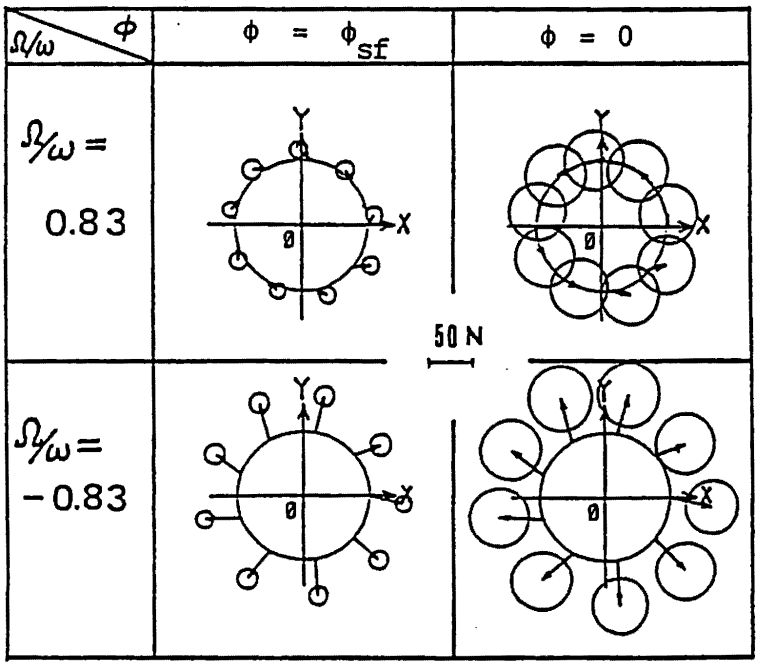

Fig. 8 Ensemble averaged fluid forces and their fluctuation

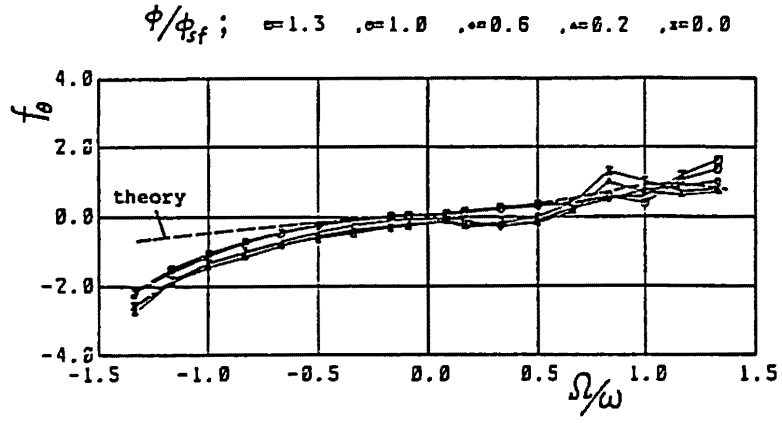

(a) Tangential component

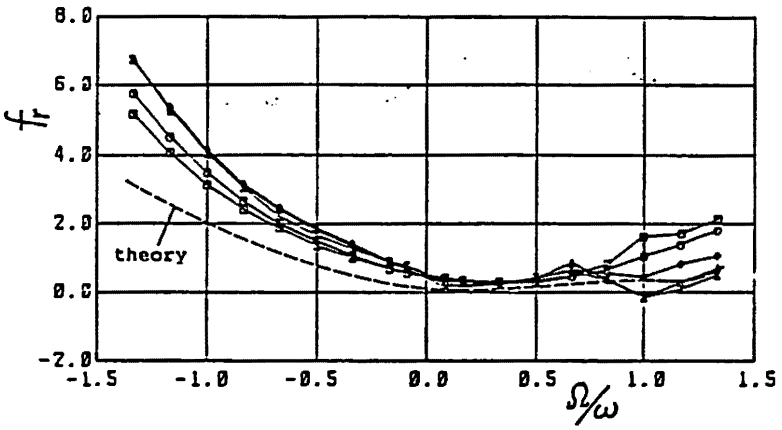

(b) Radial component

Fig. 9 Normalized fluid forces of impeller A in vaneless diffuser.

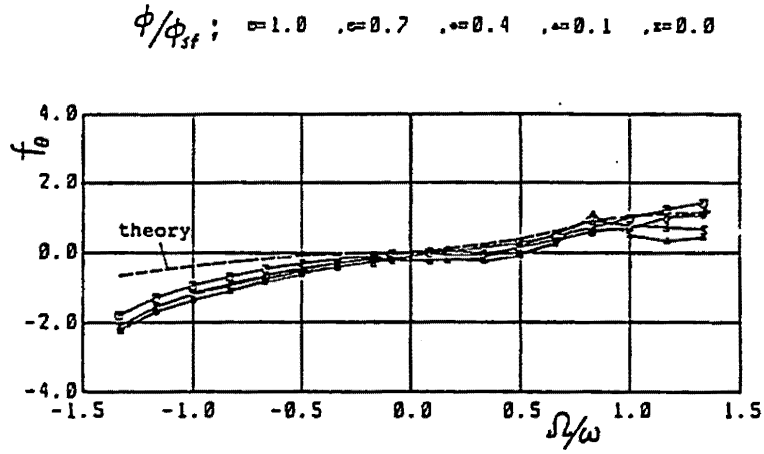

(a) Tangential component

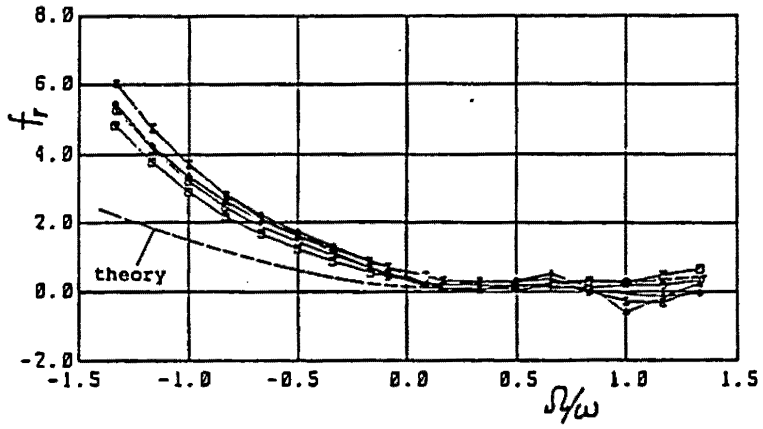

(b) Radial component

Fig. 10 Normalized fluid forces of impeller B in vaneless diffuser.

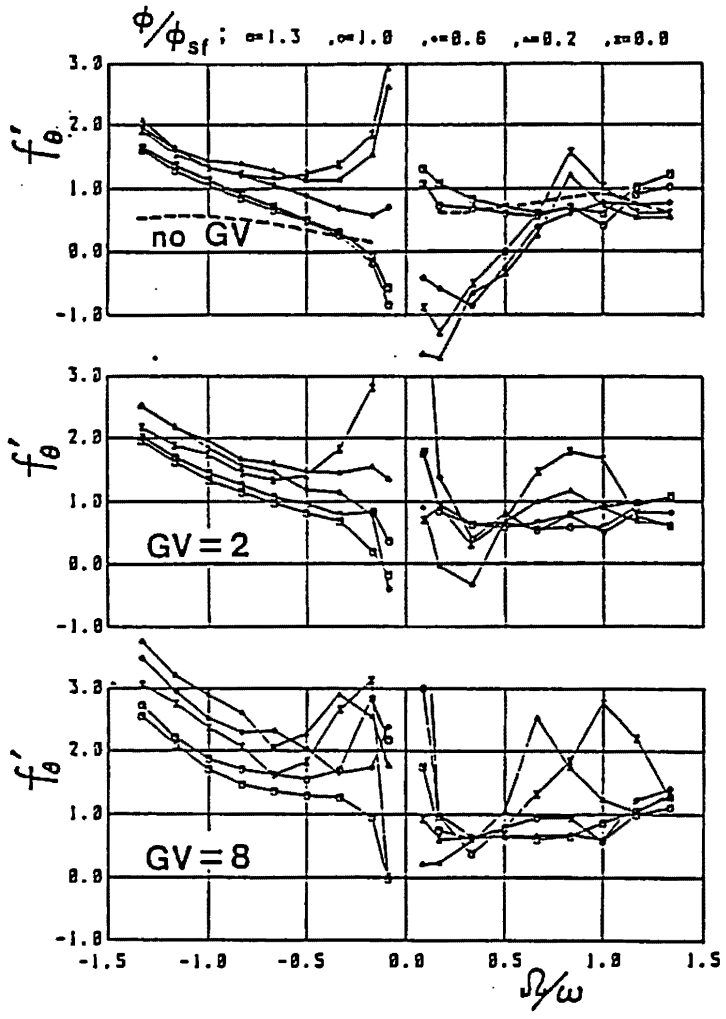

Fig.11 Effect of guide vanes on rotor stability, impeller A

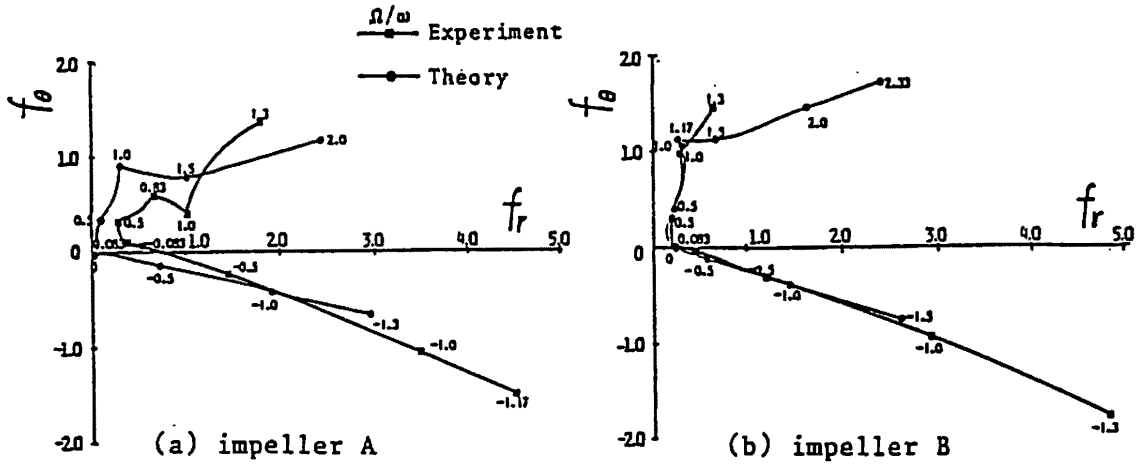

Fig. 12 Comparison between theory and experiment at shock-free entry

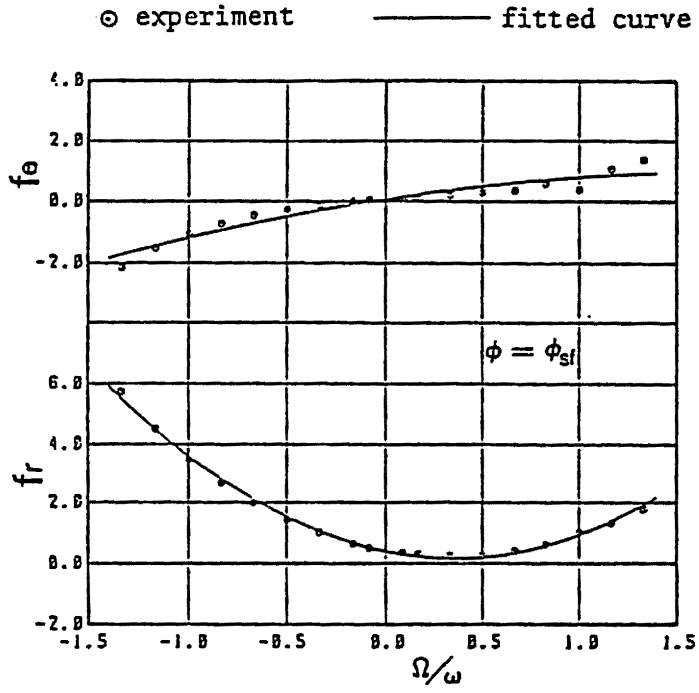

Fig. 13 Measured data and fitted curves of impeller A at shock-free entry

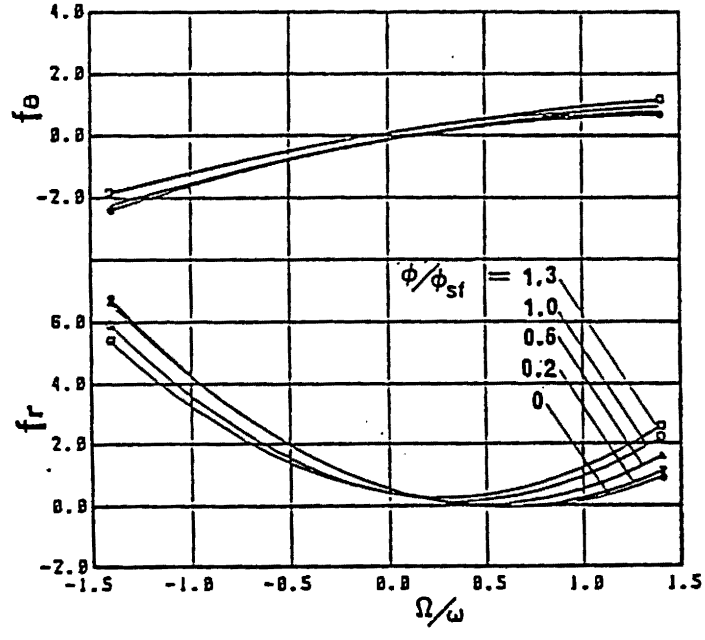

Fig. 14 Fitted curves of impeller A at various flow rate